Appl. Phys. B 71, 755–763 (2000) / Digital Object Identifier (DOI) 10.1007/s003400000384

Applied Physics B
Lasers
and Optics

Analysis of the local conformation of proteins with two-dimensional fluorescence techniques

A. Brockhinke*, R. Plessow, P. Dittrich, K. Kohse-Höinghaus

Physikalische Chemie I, Fakultät für Chemie, Universität Bielefeld, Universitätsstr. 25, 33615 Bielefeld, Germany
(Fax: +49-521/106-6027, E-mail: brockhinke@pc1.uni-bielefeld.de)

Received: 10 February 2000/Published online: 13 September 2000 –

Abstract. Two 2D fluorescence techniques are described which allow the study of conformational changes in proteins in their native form in μM solutions using aromatic amino acids (tryptophan, tyrosine) as intrinsic fluorescence markers. Simultaneous time- and wavelength-resolved fluorescence spectra are measured using a 80 ps laser source in conjunction with streak detection in the exit plane of an astigmatism-corrected spectrometer. This approach allows identification of different photophysical processes by their associated lifetime and spectral intensity distribution; errors due to the more common integration over a wider spectral range are avoided. Time-resolved spectra are sensitive to changes in the collisional environment (dynamic quenching) and can thus be used to monitor local conformation changes close to the respective fluorophors. This is demonstrated for the Ras protein which undergoes a drastic conformation change while binding to different nucleotides.

Excitation-emission spectra are two-dimensional fluorescence images with one axis corresponding to the excitation and the other to the emission wavelength. Thus, they contain all conventional excitation and fluorescence spectra of a given substance. The 2D structure facilitates the interpretation of these spectra and allows the direct identification of resonance effects, scattering and the isolation of the contribution of different fluorophors to the complete spectrum. This is demonstrated for mixtures of tyrosine and tryptophan. In this case, both wavelength-resolved spectra and temporal decays are affected by energy transfer processes between the two amino acids.

In a last example, both static and time-resolved spectral methods are combined to determine the respective contribution of static and dynamic quenching in calsequestrin. Evaluation of the fluorescence data is in good agreement with a recent crystallographic analysis which shows that all tryptophans are located in a conserved domain of the protein. Addition of Ca^{2+} ions leads to a more compact form of calsequestrin and to polymers. This information would not be obtainable from either of the two techniques alone.

PACS: 87.15.Mi; 78.47.+p; 33.50.j; 42.62.Be

Of the techniques employed for the analysis of biochemical and biological structure and function, many are of spectroscopic nature [1], a common advantage being their potential non-invasivity. Fluorescence spectroscopy in particular, due to its high sensitivity and selectivity, has found widespread application for the study of structural parameters and intramolecular interactions [2, 3]. In recent years, the main interest in using fluorescence spectroscopy in biochemical research has been devoted to time-resolved investigations [4], since static or "average" information on the complex structure of proteins and molecular assemblies may result in misleading interpretation, their functions being often dependent on conformational changes and structural fluctuations [1]. Depending on the specific dynamic rearrangement process from rapid molecular vibration to segmental or global motion, an impressive time span of the order of picoseconds to seconds may need to be covered [2, 4].

Aromatic amino acids, and most specifically tryptophan, have been used as intrinsic fluorescence probes in numerous studies [2, 4]. The complexity of fluorescence emission in cases where multiple tryptophans are present in the investigated protein [5] has encouraged further systematic investigation of the photophysics of tryptophan and indole systems [6, 7], including the detailed study of individual rotamers or substrates [8–10], the high sensitivity of tryptophan fluorescence to the local environment being a sensitive indicator of dynamic processes on the molecular scale [3, 7]. In combination with site-directed mutagenesis [4, 11, 12], single-tryptophan mutants have been used to provide a site-specific response.

Typical time-resolved tryptophan fluorescence experiments with sub-nanosecond time resolution employ syn-

*Corresponding author.

Dedicated to Professor Jürgen Wolfrum on the occasion of his 60th birthday.

chrotron [5] or laser [13, 14] excitation in combination with photon counting detection techniques. Polarization-sensitive fluorescence detection is often used to gather information on rotational motion by investigation of the anisotropy decay. While temporal resolution is thus ensured, most experiments provide fluorescence information at a single or a few individual emission wavelengths, where bandpass filters may often be used in a wavelength-integrative manner to ensure high photon count rates [15–18]. Important information, i.e. on the detailed photophysical processes responsible for the emission, may be lost by this approach. This has been demonstrated by several researchers [5, 13, 14], who have observed a pronounced change of fluorescence lifetime with wavelength which may devalue results measured at a single emission wavelength or with broadband filters [5].

In the present investigation, a novel approach providing simultaneous time and wavelength resolution is demonstrated in picosecond laser fluorescence experiments using tryptophan as intrinsic probe. This two-dimensional approach provides direct correlations between the temporal and spectral fluorescence behavior. In addition, a second two-dimensional technique is used, excitation-emission spectroscopy, which provides complementary information and allows us to detect energy transfer processes. With a combination of these two powerful approaches, four independent discriminative variables are addressed which govern the photophysical processes – excitation and emission wavelength as well as intensity and temporal decay, and unparalleled information is obtained from the observed correlations. To demonstrate the potential of these techniques, several examples are given in biochemical systems which have been well investigated before. Conformational rearrangements are observed in an experiment involving the Ras protein and several nucleotides, energy transfer is studied in tryptophan/tyrosine mixtures, and static and dynamic quenching is investigated in calsequestrin at different Ca^{2+} concentrations.

1 Experimental

1.1 Time- and wavelength-resolved measurements

Time-resolved measurements are performed using a short-pulse laser system in conjunction with an intensified streak camera. The laser system (Spectra Physics) consists of a Ti:sapphire laser (Tsunami) pumped by a 7-W Ar^+ laser. It is capable of producing pulses with either 3 ps or 80 ps duration in the near infrared (between 750 and 900 nm) with a repetition frequency of 80 MHz, individual pulses have an energy of approximately 10 nJ. For the present application, 80-ps pulses with considerably higher energy in the UV are desired. A regenerative amplifier TSA-50 and two linear amplifiers are used; they are pumped with the second-harmonic radiation of two Nd:YAG lasers. With amplification factors of 10^5, 2.5 and 4, respectively, the resulting pulses have typical energies of 15 mJ at about 850 nm and a repetition rate of 10 Hz. Consecutive frequency-doubling and mixing of the second harmonic with the fundamental wavelength provides UV radiation tunable between 250 nm and 300 nm. For the experiments described in this paper, wavelengths near 280 nm are used; the pulse length was 80 ps, and a bandwidth of about $0.7\,cm^{-1}$ and energies between 1 mJ and 2 mJ are reached. From this, between 50 μJ and 250 μJ are split off by a quartz plate and are used for the actual measurements; the remainder is directed to an energy meter and serves as reference for the pulse energy. The temporal shape of the pulse is obtained with an autocorrelator, and the wavelength position is controlled with a dual-bandwidth wavemeter (Burleigh). A more detailed description of the optical setup can be found elsewhere [19, 20].

The fluorescence emission is collected with a spherical mirror ($f = 250$ mm, $d = 250$ mm) to avoid chromatic aberrations when using a large spectral detection range. A cut-off filter (Schott WG 320, 3 mm) at 320 nm is used to block Rayleigh scattering and scattered light from optical surfaces. The emission is spectrally dispersed with a 275-mm imaging spectrometer (Acton Research Corp., SpectraPro 275i) with a 150-l/mm grating (blaze wavelength 500 nm). Temporal resolution is achieved with a streak camera (Hamamatsu C2830), the output of which is amplified by a MCP, imaged on a phosphor screen and coupled to a CCD camera (C4880) where the data is stored and transmitted to a computer. The image detected by the streak camera has a size of 1000×1018 pixels, it is decoded by the HPD-TA software supplied by Hamamatsu. Available time intervals are 0.5, 1, 2, 5, and 10 ns.

1.2 Calibration and evaluation of time-resolved spectra

For a typical fluorescence measurement using the picosecond laser/streak camera setup, the emission of 1800 consecutive laser pulses is integrated corresponding to a time period of 3 min for each experiment. From each measurement, a two-dimensional image is obtained with a time and a wavelength axis; intensities are stored with 16 bit resolution by the CCD chip. The time and wavelength axes correspond to the selected spectrometer dispersion and streak interval; for most of the experiments, a wavelength range of 200 nm ($\lambda_{em} = 300$–500 nm) and a time interval of 10 ns is chosen. The wavelength span and the absolute spectral position are determined using a Hg calibration lamp and Rayleigh and Raman scattering with different excitation wavelengths between 250 and 350 nm; the Raman signature of water (Raman shift of $3450\,cm^{-1}$) is used as a reference in all images. Since the efficiency of the spectrograph grating (blaze 500 nm) and of the camera are not constant over this large wavelength region, a calibration is performed using a deuterium lamp, and a halogen lamp with a blackbody temperature of 3200 K. To investigate potential damaging effects on the biomolecular samples by the irradiation of laser light, a series of experiments is conducted with attenuating the laser beam by one order of magnitude. Also, measurements are performed repeatedly with the same sample. No indication of deterioration of the samples is found in any experiment.

Two-dimensional raw data images are processed by assigning the corresponding time and wavelength scales. Background luminescence is measured with the respective pure buffer solution and subtracted from the fluorescence images. Furthermore, a smoothing procedure is used averaging information from 3×3 pixels. To account for the wavelength dependence of the detection efficiency, the images are divided by the appropriate calibration file. For the evaluation of spectra and of temporal decays from the processed fluorescence

images, cross sections are taken through the image keeping either temporal or spectral range constant. For temporal profiles, the spectral bandwidth is typically taken to be 5–10 nm. Fluorescence decays are evaluated using a bi-exponential fit

$$I(t) = \sum_{i=1}^{2} \alpha_i \mathrm{e}^{-t/\tau_i} \,. \tag{1}$$

Here, $I(t)$ is the time-dependent fluorescence intensity, and α_i is the amplitude corresponding to τ_i. The detected signal $F(t)$ results from a convolution of the fluorescence intensity $I(t)$ and the temporal profile of the exciting laser pulse, $P(t)$

$$F(t) = \int_0^t P(t')\, I(t-t')\mathrm{d}t' = P(t) \otimes I(t) \,. \tag{2}$$

In principle, the temporal decay of the fluorescence may be obtained by deconvolution. However, this procedure is of questionable success if the signal-to-noise level is non-negligible. Therefore, we have used the method of numerical reconvolution. For this, the pulse profile $P(t)$ is convoluted with an estimated function, and the resulting $F(t)$ is iteratively fitted to the signal $I(t)$ by minimizing χ^2:

$$\chi^2 = \sum_{i=1}^{x} \frac{(I(t_i) - F(t_i))^2}{\sigma_i^2} \,, \tag{3}$$

with $I(t_i)$ being the individual data points. The standard deviation σ_i for each data point may be estimated from Poisson statistics with $\sigma_i = \sqrt{I(t_i)}$. For minimizing χ^2, the routine of Marquardt and Levenberg [21] is used. As a suitable criterion for the quality of the fit, the weighted residual $R(t)$ is determined according to

$$R(t_i) = \frac{I(t_i) - F(t_i)}{\sqrt{I(t_i)}} \,. \tag{4}$$

A numerical fitting routine for multidimensional fluorescence data following [22] is employed. A typical time-resolved fluorescence signal is shown in Fig. 1 together with the pulse profile and the bi-exponential fit. The lower trace shows the weighted residual. Since this residual is unstructured, it can be concluded that this fit is sufficient to describe the observed fluorescence decay curve. In this case, two lifetimes of $\tau_1 = 2710 \pm 80$ ps and $\tau_2 = 340 \pm 40$ ps are deduced. Errors are determined with a rigorous error analysis [23] in a confidence interval of 97.7% (2σ). The insert in Fig. 1 shows the contribution of the component with the longer lifetime (shaded area) in comparison to that of the short-lived process. It can be seen, that the fluorescence is dominated by the long-lived process (total contribution 87%).

Recently, Wasylewski et al. [11] demonstrated that simple bi-exponential fits are not always adequate to describe the fluorescence spectra for wavelength integrated measurements. Instead, they use fits to one or two continuous Gaussian distributions for the lifetime components. Other authors suggest using up to four discrete lifetimes [24–26]. However, tests for several of the fluorescence spectra evaluated for this paper showed that in our case the quality of the fit does not significantly improve by introducing Gaussian- or Lorentzian-shaped distributions. In many cases the opposite was true:

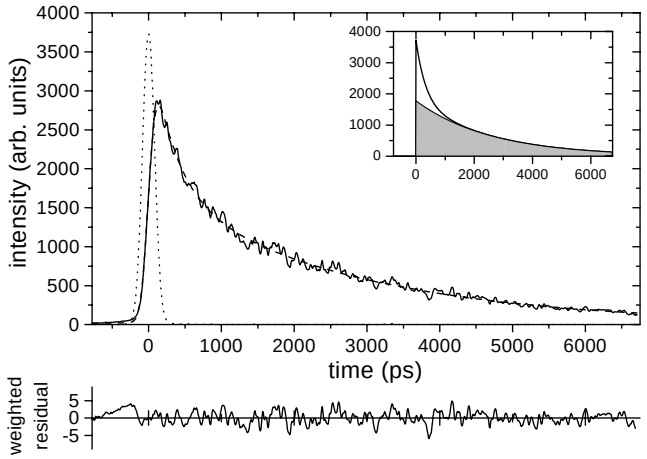

Fig. 1. Time-resolved fluorescence decay curve for calsequestrin ($[Ca^{2+}] = 0.7$ mM) at detection wavelength $\lambda_{em} = 340$ nm (*solid*), laser pulse (*dotted*) and fit to a bi-exponential model (*dashed*). The graph at the bottom is the weighted residual. The *insert* shows the contribution of the component with the longer lifetime (*shaded area*) in comparison to that of the short-lived process

due to the increasing number of free parameters the fit is not as stable as before and the accuracy generally drops. Additionally, it should be pointed out that numerical reconvolution is only one method to recover lifetimes from experimental spectra. Frequently, the maximum entropy method (MEM) is used [27–29] which is supposed to be more stable and less affected by the initial parameters. However, for high-quality data both MEM and reconvolution techniques will yield the same results. A detailed comparison of these methods can be found in Hof et al. [30].

1.3 Excitation-emission spectra

In order to get more complete information about the fluorescence process, excitation-emission spectroscopy is used here as a second two-dimensional fluorescence technique in conjunction with time-resolved spectroscopy. The setup to acquire excitation-emission spectra (EES) is similar to that employed in commercial static fluorimeters: the output of a continuous Xe-lamp (75 W, LOT Oriel) is wavelength-separated by a first monochromator (Spectra Pro ARC-175, 1800 l/mm grating, blaze 250 nm) and then used to irradiate a sample. The fluorescence is collected by mirror optics at right angles and imaged on the entrance slit of a second spectrometer while compensating astigmatism at the same time. The signal is detected by an intensified CCD camera (Theta systems, 286×384 pixels) in exit plane of the spectrometer. The resulting images are spatially and spectrally resolved. As the next step, one averaged fluorescence spectrum is calculated from the raw images and stored in the computer. This process is repeated for different excitation wavelengths. The result is a two-dimensional fluorescence pattern with the y axis corresponding to the excitation, and the x axis to the emission wavelength. Sample spectra are presented later (Fig. 4).

For the experiments reported here, the width of the monochromator slits are chosen so that both the bandwidth of the exciting radiation and the resolution of the detection spectrograph are 4 nm. The wavelength range is

$\lambda_{ex} = 240$–300 nm (in 0.5-nm increments) for the UV light and $\lambda_{em} = 240$–500 nm for the detector. The time to acquire a complete EES is typically less than 15 min. Post-processing of the EES includes subtraction of the dark current background, 3×3 smoothing to reduce noise, conversion of pixel to wavelength scales, and multiplication with a reference file to take the varying lamp intensity as well as grating and detection efficiency into account.

One EES file contains the complete excitation and emission spectra of a given substance. Post-processing allows the recovery of the fluorescence spectra at different excitation wavelengths (corresponding to horizontal profiles in the EES) as well as to determine excitation spectra at different emission wavelengths with an arbitrary bandpass (corresponding to vertical profiles averaged over a given region).

One major advantage of EES in comparison to the standard one-dimensional spectra is that they facilitate interpretation. Raman and Rayleigh scattering lead to tilted lines in the spectra and are thus easily identified. For large molecules in solution, the energy is usually dissipated rapidly (internal conversion) so that the major part of the fluorescence stems from the vibrational ground state of the excited molecule. In this case, the shape of the spectra for a single substance will change little during the variation of the excitation wavelength. For mixtures of fluorophors such as encountered in most proteins, however, distinct changes in the spectra will occur as soon as the excitation wavelength hits or leaves absorption bands of the different fluorophors. Resonance effects such as the direct excitation of single molecular levels will lead to separated "islands" in the spectrum and may thus be easily identified [31].

1.4 Sample preparation, reference measurements

For all measurements, samples are contained in quartz cuvettes of 10×10 mm (Hellma type 111-QS, suprasil, optical precision). They are prepared with tri-distillated water and p.a. grade chemicals. The concentration of the Ras protein in solution is 10 μM using a buffer of 50 mM tris/HCl (100 mM NaCl, 5 mM $MgCl_2$), pH 7.4. In the mixtures of tyrosine and tryptophan, the Trp concentration is kept constant at 10 μM. A 0.47 μM calsequestrin solution is prepared in a MOPS/tris buffer (50 mM) with a pH of 7.1. The Ca^{2+} concentration is modified by sequential additions of small volumes of concentrated standard solutions of $CaCl_2$.

For reference purposes and to check the calibration of the EES setup, static fluorescence is also recorded using a 150-W Xe high pressure lamp in a Hitachi F4010 spectrometer. Additionally, absorption is measured with a UV/VIS double-path spectrometer (Kontron UVIKON 860), using the buffer as a reference.

2 Results and discussion

2.1 Conformational changes in proteins

To demonstrate the advantages of simultaneous time- and wavelength-resolved fluorescence spectroscopy, we present ps-LIF measurements on the Ras protein, a system which is already well characterized by other methods [32, 33]. Ras may be regarded as a molecular switch protein relaying mitogenic signals to transcription factors localized in the nucleus as well as to cytosolic targets. The biological activity of Ras is controlled by binding to different nucleotides: many different effector molecules are known to specifically interact with the active GTP-bound form of Ras and to become activated thereby [34]. Likewise, the closely related Rap and R-Ras proteins can also bind to these effectors [35]. In contrast, the GDP form is inert. Due to its prominent role in signal transduction, mutated Ras is found in 30% of all human tumours; the mutated form is typically disabled in its GTP-hydrolytic activity and therefore cannot be switched off. In the wild type, Ras contains no tryptophan and seven tyrosines. Especially suited for fluorescence studies is a mutant form of Ras where the tyrosine at position 32 of the protein chain is substituted by a tryptophan. This position is known to be part of the effector region for RBD which undergoes a pronounced conformational change when nucleotides are exchanged from GTP to GDP.

Figure 2 shows simultaneously time- and wavelength-resolved fluorescence spectra for RasY32W.GppNHp (top) and RasY32W.GDP (bottom). GppNHp is an analog of GTP that does not undergo hydrolysis and is therefore especially well suited for investigations. In Fig. 2, the fluorescence wavelength is plotted on the *x* axis whereas the *y* axis corres-

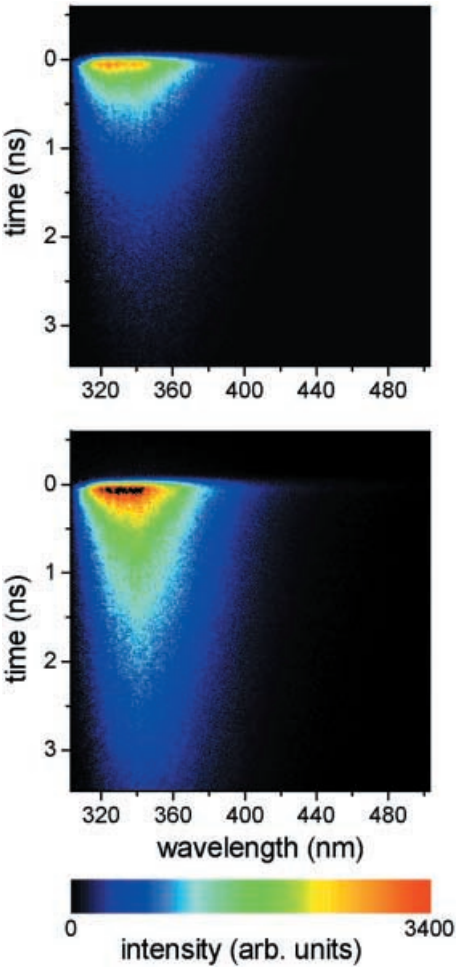

Fig. 2. Simultaneously time- and wavelength-resolved fluorescence spectra for RasY32W.GppNHp (*top*) and RasY32W.GDP (*bottom*)

ponds to the time relative to the initial laser pulse at $t = 0$. Intensities are given in a false color representation and are not normalized in this case. A comparison of these images shows striking differences: for the active GppNHp form, the fluorescence intensity is smaller and falls off more rapidly than for the inactive GDP form. For a more detailed analysis, vertical profiles have been taken from these images in 10-nm increments, which are then fitted to a bi-exponential model using the reconvolution procedure outlined above. The results of this analysis are summarized in Fig. 3. In the top part, the wavelength dependence of the fluorescence lifetime is shown. Whereas the lifetimes of the short process are always similar with values around $\tau_2 \approx 300$ ps, pronounced differences can be seen for the long-lived component. For RasY32W.GppNHp, the lifetime τ_1 is less than 1.4 ns for an excitation wavelength of $\lambda_{ex} = 320$ nm. Thereafter, τ_1 increases and reaches a plateau at $\tau_1 = 2.0$ ns for $350 < \lambda_{ex} < 410$ nm and rises again to 2.5 ns for longer wavelengths. In contrast, the lifetime starts at $\tau_1 = 2.0$ ns for the GDP form of Ras and rises rapidly to values in excess of 4.0 ns for longer wavelengths. This shows, that active (GTP) and inactive (GDP) form of Ras can be distinguished by the fluorescence lifetime with a high reliability. The difference in lifetimes is larger by a factor of 10 than the error margin for the determination of τ_1 (which already corresponds to a 2σ confidence interval).

In the bottom part of Fig. 3, decay-associated spectra are plotted. Intensities in these spectra are calculated by evaluating the expression $\alpha_i \tau_i$ and thus represent the contribution of the respective process to the total fluorescence intensity. It can be seen that the fluorescence is dominated by the process with the long lifetime in all cases. For both protein forms, the maximum intensity is reached around $\lambda_{em} = 345$ nm, close to that for a sample of pure tryptophan (cf. Figs. 4 and 5 and the description in the next section). In contrast, the peak intensity of the part of the fluorescence associated with the short lifetimes is shifted towards lower wavelengths (around $\lambda_{em} = 325$ nm).

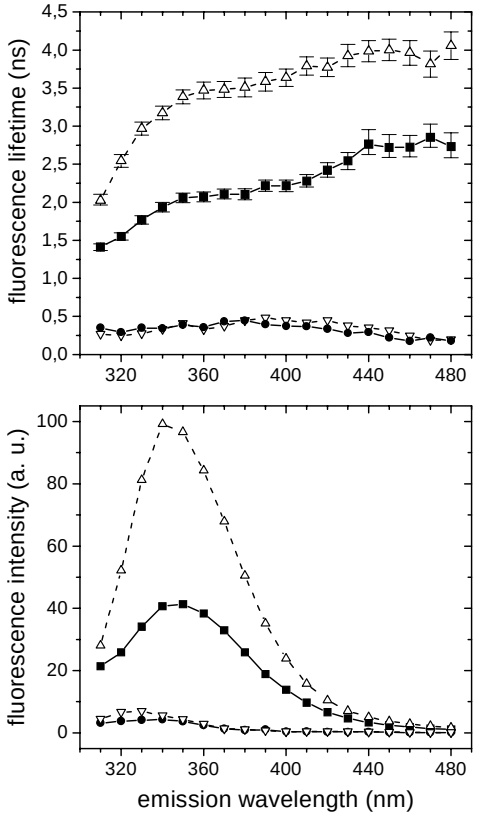

Fig. 3. *Top*: wavelength-dependence of the fluorescence lifetimes τ_1 and τ_2 for RasY32W.GppNHp (*solid*, τ_1: *square*, τ_2: *circle*) and RasY32W.GDP (*dotted*, τ_1: *open up triangle*, τ_2: *open down triangle*). *Bottom*: decay-associated emission spectra

It should be noted, that the longer lifetime changes significantly close to the maximum of the emission: in the interval marked by the FWHM of the fluorescence spectrum, it rises from 1.5 to 2.1 ns for RasY32W.GppNHp and from 2.5 to 3.5 ns for Ras.GDP. This demonstrates one important advantage of simultaneous time- and wavelength-resolved measurements in that contributions by several photophysical processes may be recognized and treated individually. The wavelength integration intrinsic of conventional bandpass methods would inevitably lead to a more complex behavior of the fluorescence decay curve which then would have to be fitted to more complex mathematical expressions such as multi-exponential decay curves or functions with a distribution of lifetimes.

The large differences between the time-resolved spectra of both, active and inactive, forms of the Ras protein show that the local environment of the single tryptophan has changed during the exchange of GTP and GDP. Water is known to be an effective quencher of tryptophan fluorescence [36]. The relatively short lifetime of the RasY32W.GppNHp fluorescence is thus an indicator that the tryptophan is more exposed to the solvent than in the GDP-bound form. This interpretation is in line with a crystallographic analysis [32, 33]. In addition to the drastic changes in the time-resolved spectra of the active and the inactive form described above, it is even possible to use this technique to detect the minor conformational changes induced by different GTP-analogs (GppNHp, $GppCH_2p$ and GTPγS) which are otherwise very similar [37].

This example shows that time-resolved analysis of fluorescence spectra provides information that can be used to distinguish proteins and to follow local conformation changes in solution. Among the aromatic amino-acids, tryptophan is especially well suited as a sensor since its fluorescence properties are quite sensitive to changes in environment. Advantages of the lifetime spectra over conventional spectra are that they are independent on concentration and energy fluctuations. Thus, they are better suited to follow reactions such as the nucleotide exchange in the Ras protein than standard fluorescence methods [38]. Additionally, time-resolved anisotropy measurements are possible using the setup described above in conjunction with polarization prisms for the laser and the signal beam. They provide additional information on the local flexibility of fluorophors and the global re-orientation of the molecule [15–17, 20].

2.2 Energy transfer processes

Since it would be of interest to use both tryptophan and tyrosine simultaneously as intrinsic protein fluorophors, mixtures of tryptophan and tyrosine have been investigated in order to study whether a separation of the fluorescence contributions

of both species is possible and how the spectra and the temporal evolution of the signal intensities are affected by energy transfer processes. Figure 4 shows excitation-emission spectra of two tryptophan/tyrosine mixtures with a concentration ratio of 1 : 2 (top) and 1 : 5 (bottom). Common feature in both spectra is the strong tilted line which arises from Rayleigh scattering. On the longer wavelength side, this line is accompanied by another fairly weak line corresponding to vibrational Raman scattering on water (Raman shift 3450 cm^{-1}, at $\lambda_{ex} = 300$ nm this amounts to a shift of $\Delta\lambda = 35$ nm). By subtracting the EES of a buffer solution instead of only the dark-current background as in Fig. 4, a complete suppression of both, Rayleigh and Raman lines is possible.

In comparing both images in Fig. 4, it is evident that the fluorescence intensity becomes more intense for excitation wavelengths from $\lambda_{ex} = 240$ to 285 nm for the tyrosine-rich mixture, with the dominant contribution being in the interval 280 nm $\leq \lambda_{em} \leq$ 320 nm (where tyrosine is known to emit radiation). In contrast, at $\lambda_{ex} \geq 290$ nm the fluorescence spectra do not change significantly from Figs. 4a to 4b, since the concentration of tryptophan was held constant in both mixtures. Evaluation of the EES at $\lambda_{ex} = 290$ nm (only tryptophan fluorescence visible) and at a different $\lambda_{ex} \leq 290$ nm (where both, tryptophan and tyrosine molecules are excited) can be used to separate the contribution of the two fluorophors in the complete spectrum. It is easily imagined from this example that EES will be different for different proteins (dependent on the number and the local environment of the aromatic amino acids) and may thus be used as a 'fingerprint' of the substance. Additionally, the intensity variations visible in the EES can be used to investigate static quenching (this is described in the next section); calibration of the intensity axis allows the determination of quantum yields. As an example of a more quantitative analysis of EES, conventional fluorescence spectra have been extracted at $\lambda_{ex} = 280$ nm for the 1 : 5 tryptophan/tyrosine mixture and are compared with the spectra of the pure amino acids in Fig. 5. Tyrosine emits mainly in the interval 280 nm $\leq \lambda_{em} \leq$ 320 nm, whereas tryptophan fluorescence is significantly stronger and is concentrated around 325 nm $\leq \lambda_{em} \leq$ 375 nm. However, the spectrum of the mixture of the two amino acids is not a simple addition of the respective spectra of the molecules. Tyrosine fluorescence is diminished by 20% whereas tryptophan fluorescence is significantly stronger as expected. These changes are due to energy transfer which can occur since the absorption spectrum of tryptophan partially overlaps the fluorescence spectrum of tyrosine. The Förster distance for this transfer is 14 Å with the quantum yield of the donor of approximately 0.04 [39–42].

In a simplified two-level model, this energy transfer may be described by the following differential equations:

$$\frac{\mathrm{d}N_\mathrm{Y}}{\mathrm{d}t} = -(k_\mathrm{Y} + k_\mathrm{ET})N_\mathrm{Y}\,, \qquad (5)$$
$$\frac{\mathrm{d}N_\mathrm{W}}{\mathrm{d}t} = k_\mathrm{ET}N_\mathrm{Y} - k_\mathrm{W}N_\mathrm{W}\,.$$

Here, N is the number of excited molecules, and k the rate constant, with the subscripts Y and W indicating tyrosine and tryptophan, respectively. k_ET is the rate constant for energy transfer between the two excited states. For long emission wavelengths where all fluorescence stems from tryptophan alone, this equation system has the following solution:

$$I(t) = C_1 N_\mathrm{W} = -A_1 \mathrm{e}^{-t/\tau_1} + (A_1 + A_2)\mathrm{e}^{-t/\tau_\mathrm{W}}\,. \qquad (6)$$

That is, the resulting fluorescence may still be described by a bi-exponential decay, but now one of the associated amplitudes will be negative. This results in a curve that rises first (due to energy transfer), reaches a maximum and then starts to drop off. The relaxation times may be calculated according to $\tau_1 = 1/(k_\mathrm{Y} + k_\mathrm{ET})$ and $\tau_\mathrm{W} = 1/k_\mathrm{W}$. Figure 6 shows the time-resolved fluorescence decay for the

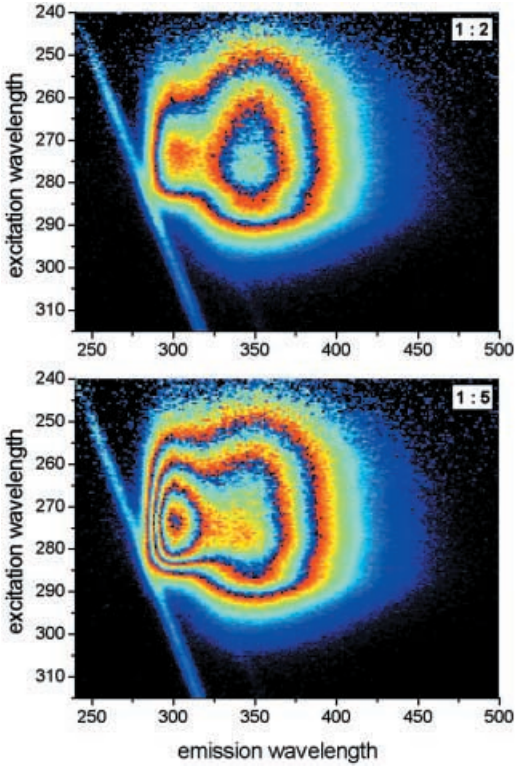

Fig. 4. Excitation-emission spectra of two tryptophan/tyrosine mixtures. Concentration ratio 1 : 2 (*top*) and 1 : 5 (*bottom*)

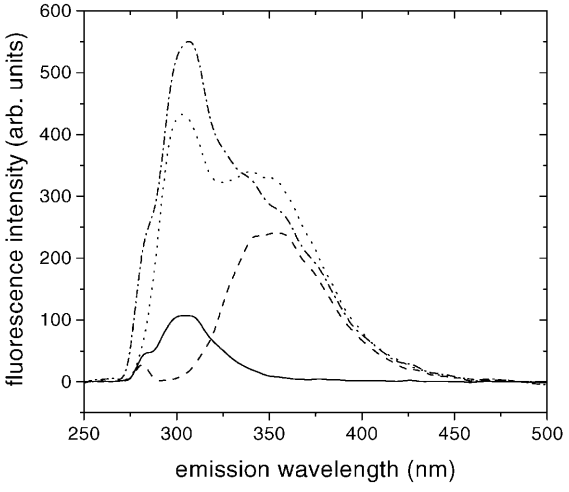

Fig. 5. Fluorescence spectra of tryptophan (*dashed*), tyrosine (*solid*) and 1 : 5 mixture (*dotted*) at excitation wavelength $\lambda_{ex} = 280$ nm. Also shown is the calculated spectrum of the mixture (*dashed dotted*)

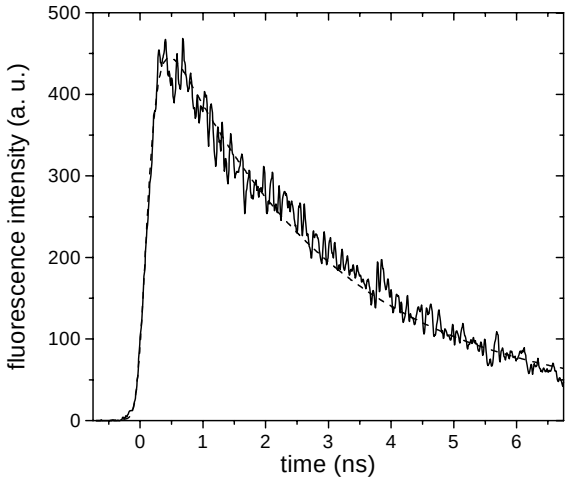

Fig. 6. Time-resolved fluorescence decay curve for a 1 : 5 Trp/Tyr mixture at $\lambda_{ex} = 280$ nm and $\lambda_{em} = 420$ nm. Experimental data are fitted to a bi-exponential model which yields $\tau_1 = 2.75$ ns, $\alpha_1 = 597$ and $\tau_2 = 130$ ps, $\alpha_2 = -598$

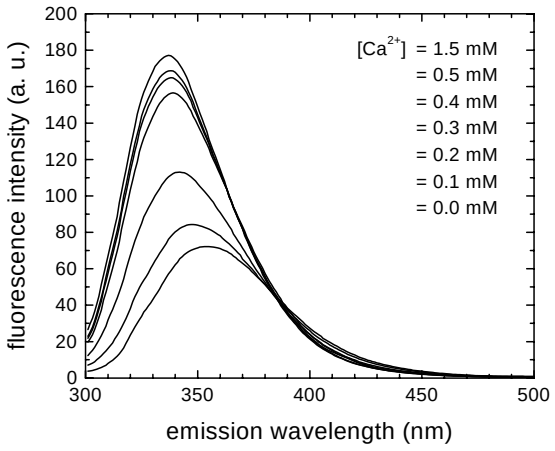

Fig. 7. Fluorescence spectra of phospho-calsequestrin at different Ca^{2+} concentrations. The peak intensity increases with increasing Ca^{2+} concentration

1 : 5 tryptophan/tyrosine mixture at the emission wavelength $\lambda_{em} = 420$ nm. As can be seen in Fig. 5, all fluorescence is due to tryptophan at this position. A fit of the observed decay to a bi-exponential model yields $\tau_1 = 2.75$ ns, $\alpha_1 = 597$ and $\tau_2 = 130$ ps, $\alpha_2 = -598$. The first process clearly dominates the fluorescence, its lifetime is close to that of pure tryptophan at this particular wavelength. The process with the negative amplitude is with 5% of minor importance for the overall fluorescence; its lifetime is dominated by the rate of energy transfer between the excited states of tyrosine and tryptophan.

Finally, it should be noted that energy transfer from tyrosine to tryptophan is only one aspect influencing the fluorescence properties of proteins. For example, the ratio between the number of tryptophan and tyrosine residues of Ras is 1 : 8 and thus higher to that of the mixture investigated in Figs. 4 and 5. However, tyrosine fluorescence is diminished even further inside of the Ras protein than in the mixture of the pure amino acids. This is due to additional quenching of charged amino groups and neutral carboxylate groups that has been observed before [43–45].

2.3 Static and dynamic quenching

Calsequestrin is the most important calcium-binding protein present in the lumen of sarcoplasmatic reticulum of muscle tissue. It coordinately binds and releases up to 50 Ca^{2+} ions per molecule for each contraction–relaxation cycle by a mechanism that is not yet completely resolved [46–48]. Calsequestrin contains 11 tyrosine and 5 tryptophan residues with the Trp residues located in one domain of the protein only. The threonin residue at position 253 may by phosphorylated thus forming the phospho-calsequestrin. However, the fluorescence properties of both protein forms are identical

Figure 7 shows fluorescence spectra of phospho-calsequestrin at different Ca^{2+} concentrations. To avoid aggregation, a protein concentration of 26 μg/ml (0.47 μM) has been used. Excitation wavelength is $\lambda_{ex} = 290$ nm. It is seen that the fluorescence intensity increases by a factor of two for the sample with 0.5 mM Ca^{2+} addition; at the same time the location of the fluorescence maximum changes from $\lambda_{em} = 354$ nm to $\lambda_{em} = 338$ nm. Further addition of Ca^{2+} does not significantly change the spectrum. These results are in good agreement with earlier measurements by Hidalgo et al. [49]. They have been attributed to local conformation changes which transfer tryptophan residues from the polar surface to the hydrophobic interior of the protein [49–51].

Time-resolved measurements show that nearly all fluorescence in the LIF spectra of calsequestrin is associated with a process with a long lifetime (compare Fig. 1). Figure 8 shows a plot of the fluorescence lifetimes of calsequestrin vs. the Ca^{2+} concentration. Both, short and long lifetime remain constant for all Ca^{2+} concentrations. In consequence, the pronounced decrease in fluorescence intensity observed in Fig. 7 cannot be due to dynamic quenching as proposed by [49–51], since it would manifest in different fluorescence lifetimes. All processes that affect the intensity of fluorescence radiation but not the lifetime of the excited state are usually summarized under the term ‘static quenching’. In most cases, static quenching is due to the formation of a complex in the ground state of the molecule with either a different absorption spectrum or an excited state that undergoes non-radiative decay [36].

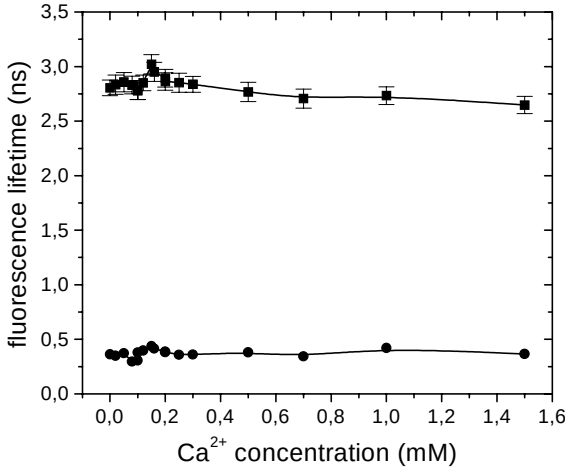

Fig. 8. Effect of Ca^{2+} on the fluorescence lifetime of calsequestrin

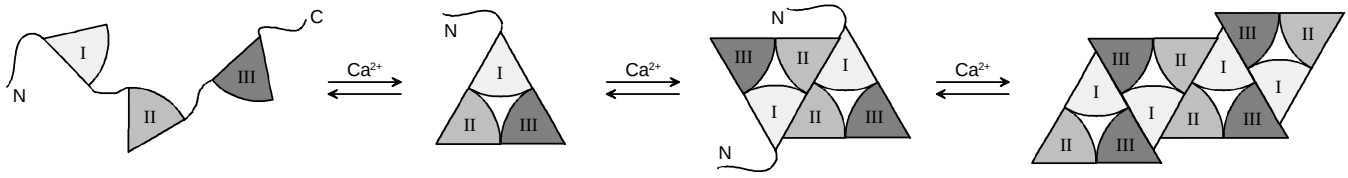

Fig. 9. Structural changes of calsequestrin at different Ca^{2+} concentrations [46]. All five tryptophan residues are located in domain III of the protein

For calsequestrin the absence of dynamic quenching shows that the local environment of the fluorophors does not change significantly. The strong static quenching is indicative of the formation of larger complexes with different absorption properties with increasing Ca^{2+} concentration. Additionally, it seems possible that the more compact tertiary structure of the protein facilitates energy transfer from the tyrosine to the tryptophan residues and thus leads to an increased fluorescence yield. Recent crystallographic measurements [46] confirm this interpretation: all tryptophan residues are concentrated in the conserved domain III of the calsequestrin. When the Ca^{2+} level increases, the three domains collapse forming a more compact protein. For even higher Ca^{2+} concentrations, polymerisation of calsequestrin monomers is observed. This mechanism is sketched in Fig. 9 following a more elaborate drawing in [46].

This example clearly shows that combination measurements using two-dimensional fluorescence techniques may help to reveal the structure of proteins.

3 Summary

Two different two-dimensional fluorescence techniques are described and used to study conformational changes of proteins. Common feature of both approaches is that proteins are investigated under physiologic conditions in μM solutions using the aromatic amino acids tryptophan and tyrosine as intrinsic fluorescence markers.

In the first approach, a tunable picosecond laser (80 ps pulse duration, 150 μJ typical energy) is used to selectively excite the chromophors. Fluorescence is detected with a streak camera in the exit plane of an astigmatism-corrected spectrometer thus allowing simultaneous time- and wavelength-resolved measurements. This approach allows the identification of different photophysical processes by their associated lifetimes and spectral intensity distributions; errors due to the more common integration over a wider spectral range are avoided. For all investigated systems, a bi-exponential fit is adequate to describe the measured wavelength-resolved temporal decay curves.

Time-resolved spectra are sensitive to changes in the collisional environment (dynamic quenching) and can thus be used to monitor local conformation changes in the vicinity to the respective fluorophors. Results are presented for the Y32W mutant of the Ras protein. Here, the lifetime of the short-lived process remains constant whereas the long lifetime τ_1 shows a pronounced wavelength-dependence. At $\lambda_{em} = 340$ nm, the long decay time is $\tau_1 = 1.9$ ns for Ras bound to the GTP analog GppNHp, in contrast to $\tau_1 = 3.1$ ns for the Ras.GDP complex. This shows that the Ras protein undergoes a drastic conformation change during nucleotide exchange, with the tryptophan residue being more exposed to the solvent in the Ras.GppNHp complex.

Mixtures of tryptophan and tyrosine are investigated using two-dimensional excitation-emission spectra (EES). Here, one axis corresponds to the excitation and the other to the emission wavelength. Thus, the EES file simultaneously contains the complete excitation and fluorescence spectra of a given substance and facilitates the identification of resonance effects and of scattering processes as well as the isolation of the contribution of the two fluorophors to the complete spectrum. It is shown that both, static and dynamic spectra are affected by energy transfer between tyrosine and tryptophan.

Using a combination of static and time-resolved measurements we conclude that static quenching is the dominant factor influencing the fluorescence spectra of calsequestrin. A detailed evaluation of the spectra is in good agreement with a recent crystallographic analysis which shows that all tryptophan residues are located in a conserved domain of the protein. The addition of Ca^{2+} ions leads to a more compact protein conformation, a structural change which is accompanied by an increase of the fluorescence yield.

In future experiments, time-resolved anisotropy measurements will be combined with the excitation-emission and dynamic spectroscopy described in this paper. They will provide additional information about the local flexibility of fluorophors and the global re-orientation of the molecule, thus allowing an even more detailed characterization of the protein structure with fluorescence methods.

Acknowledgements. The authors wish to thank Dr. Ch. Herrmann (MPI für molekulare Physiologie, Dortmund) and Dr. M. Varsanyi and Prof. Dr. L.M.G. Heilmeyer (Ruhr-University Bochum) for valuable discussions and protein samples.

References

1. L. Brand, M.L. Jonson: *Methods in Enzymology*, Vol. 246 (Academic Press, San Diego 1995)
2. J.M. Beechem: In *Methods in Enzymology*, Vol. 278, ed. by J. Brand, M.L. Johnson (Academic Press, San Diego 1997) pp. 24–49
3. J.M. Beechem, L. Brand: Annu. Rev. Biochem. **54**, 43 (1985)
4. A.R. Holzwarth: In *Methods in Enzymology*, Vol. 246, ed. by L. Brand, M.L. Johnson (Academic Press, San Diego 1995) pp. 334–362
5. A.P. Demchenko, J. Gallay, M. Vincent, H.-J. Apell: Biophys. Chem. **72**, 265 (1998)
6. K.W. Short, P.R. Callis: J. Chem. Phys. **108**, 10 189 (1998)
7. P.R. Callis, B.K. Burgess: J. Phys. Chem. B **101**, 9429 (1997)
8. P.S. Antonini, W.F. Hillen, N. Ettner, W. Hinrichs, P. Fantucci, S.M. Doglia, J.A. Bousquet, M. Chabbert: Biophys. J. **72**, 1800 (1997)
9. A. Chattopadhyay, S. Mukherjee, R. Rukmini, S.S. Rawat, S. Sudha: Biophys. J. **73**, 839 (1997)
10. K. Döring, L. Konermann, T. Surrey, F. Jahnig: Eur. Biophys. J. **23**, 423 (1995)
11. Z. Wasylewski, P. Kaszycki, M. Drwiega: J. Prot. Chem. **15**, 45 (1996)

12. R. Vos, Y. Engelborghs, J. Izard, D. Baty: Biochemistry **34**, 1734 (1995)
13. M.D. She, W.J. Dong, P.K. Umeda, H.C. Cheung: Biophys. J. **73**, 1042 (1997)
14. F. Mérola, R. Rigler, A. Holmgren, J.-C. Brochon: Biochemistry **28**, 3393 (1989)
15. A.J. Kungl, N.V. Visser, A. van Hoek, A.G. Visser, A. Billich, A. Schilk, H. Gstach, M. Auer: Biochemistry **37**, 2778 (1998)
16. L.J. Juszczak, Z.Y. Zhang, L. Wu, D.S. Gottfried, D.D. Eads: Biochemistry **36**, 2227 (1997)
17. W.C. Lam, J.M. Seifert, F. Amberger, C. Graf, M. Auer, D.P. Millar: Biochemistry **37**, 1800 (1998)
18. B.E. Jones, J.M. Beechem, C.R. Matthews: Biochemistry **34**, 1867 (1995)
19. A. Brockhinke, W. Kreutner, U. Rahmann, K. Kohse-Höinghaus, T.B. Settersten, M.A. Linne: Appl. Phys. B **69**, 477 (1999)
20. R. Plessow, A. Brockhinke, W. Eimer, K. Kohse-Höinghaus: J. Phys. Chem. B **104**, 3695 (2000)
21. W.H. Press, B.P. Flannery, S.A. Teukolsky, W.T. Vetterling: *Numerical Recipes in C* (Cambridge University press, Cambridge 1988)
22. J.R. Lakowicz: *Topics in Fluorescence Spectroscopy* (Plenum Press, New York 1991)
23. J.M. Beechem: In *Methods in Enzymology*, Vol. 210, ed. by J. Brand, M.L. Johnson (Academic Press, New York 1992) pp. 36–54
24. M. Roy, N. Periasamy: Photochem. Photobiol. **61**, 292 (1995)
25. M. Vincent, J. Gallay, A.P. Demchenko: J. Phys. Chem. **99**, 14 931 (1995)
26. J.R. Lakowicz, I. Gryczynski, H. Malak, M. Schrader, P. Engelhardt, H. Kano, S.W. Hell: Biophys. J. **72**, 567 (1997)
27. A.K. Livesey, A.K. Brochon: Biophys. J. **52**, 693 (1987)
28. M. Hof: Biochim. Biophys. Acta **1388**, 143 (1998)
29. D.S. Dijkstra, J. Broos, A.G. Visser, A. van Hoek, G.T. Robillard: Biochemistry **36**, 4860 (1997)
30. M. Hof, G.R. Fleming, V. Fidler: Proteins-Struct. Funct. Genet. **24**, 485 (1996)
31. A. Brockhinke, A.T. Hartlieb, K. Kohse-Höinghaus, D.R. Crosley: Appl. Phys. B **67**, 659 (1998)
32. E.F. Pai, U. Krengel, G.A. Petsko, R.S. Goody, W. Kabsch, A. Wittinghofer: EMBO J. **9**, 2351 (1990)
33. M.V. Milburn, L. Tong, A.M. DeVos, A. Brünger, Z. Yamaizumi, S. Nishimura, S.-H. Kim: Science **247**, 939 (1990)
34. A. Wittinghofer, C. Herrmann: FEBS Lett. **369**, 52 (1995)
35. C. Herrmann, G. Horn, M. Spaargaren, A. Wittinghofer: J. Biol. Chem. **271**, 6794 (1996)
36. J.R. Lakowicz: *Principles of Fluorescence Spectroscopy* (Plenum Press, New York 1983)
37. A. Brockhinke, R. Plessow, C. Herrmann, K. Kohse-Höinghaus: manuscript prepared for submission to Biophys. J. (2000)
38. J.R. Sydor, M. Engelhard, A. Wittinghofer, R.S. Goody, C. Herrmann: Biochemistry **37**, 14 292 (1998)
39. I.Z. Steinberg: Annu. Rev. Biochem. **40**, 83 (1971)
40. G. Weber: Biochem. J. **75**, 335 (1960)
41. G. Weber, M. Shinitsky: Proc. Natl. Acad. Sci. U. S. A. **65**, 823 (1970)
42. P.G. Wu, E. James, L. Brand: Biophys. Chem. **48**, 123 (1993)
43. H. Edelhoch, R.L. Perlman, M. Wilchek: Biochemistry **7**, 3893 (1968)
44. G. Weber, K. Rosenheck: Biopolymers Symp. **1**, 333 (1964)
45. R.W. Cowgill: In *Biochemical Fluorescence Concepts*, ed. by R.F. Chen, H. Edelhoch (Marcel Dekker, New York 1976) pp. 441–486
46. S.R. Wang, W.R. Trumble, H. Liao, C.R. Wesson, A.K. Dunker, C.H. Kang: Nature Struc. Biol. **5**, 476 (1998)
47. V. Shoshan-Barmatz, I. Orr, S. Weil, H. Meyer, M. Varsanyi, L.M.G. Heilmeyer: Biochim. Biophys. Acta **1283**, 89 (1996)
48. C. Szegedi, S. Sarkozi, A. Herzog, I. Jona, M. Varsanyi: Biochem. J. **337**, 19 (1999)
49. C. Hidalgo, P. Donoso, P.H. Rodriguez: Biophys. J. **71**, 2130 (1996)
50. N. Ikemoto, G.M. Bhatnagar, B. Nagy, J. Gergely: J. Biol. Chem. **247**, 7835 (1972)
51. N. Ikemoto, B. Nagy, G.M. Bhatnagar, J. Gergely: J. Biol. Chem. **249**, 2357 (1974)